PERFORMANCE PREDICTION OF THE STRUCTURAL RESPONSE OF A LARGE-SCALE THERMOPLASTIC AM PART: MODELING AND VALIDATION

George Scarlat[1*], Kyle Warren[1]

[1] Advanced Structures and Composites Center, University of Maine, Orono, Maine, USA
https://composites.umaine.edu/
* george.scarlat@composites.maine.edu

Keywords: Additive Manufacturing, Large-Scale, Fibre-Filled Thermoplastics, Structural Prediction

ABSTRACT

A framework for developing a predictive Finite-Element (FE) model for a large-scale Additively Manufactured (AM) thermoplastic structure, based on material characterization tests at coupon level, is presented in this paper. The response of interest was the monotonic loading up to the brittle structural failure. A classical elastic-plastic material using the Hill anisotropic yield criterion was used within the Abaqus FE commercial software and the predicted results compared very well with the tests, both at the coupon level as well as at the structural component level.

1 INTRODUCTION

Advances in Additive Manufacturing techniques make possible now the manufacturing of very large-scale structures. At the Advanced Structures and Composites Centre (ASCC) of University of Maine, short carbon fibres or cellulose nano-fibres with a thermoplastic material base were being used, for example, to 3D-print an 8 meters long boat hull and a 600 sqf single-family home, respectively. The boat hull was printed as a monolithic part, while the house had all the walls, floors, and roof 3D-printed and assembled in few large modules.

With larger and larger AM structures becoming a reality nowadays, the need for evaluating and predicting their structural performance takes on a new importance. In this sense, several sets of large-scale beams were 3D-printed at ASCC using a Short Fibre Reinforced Polymer (SFRP) material, on a Cincinatti BAAM 3D-printer. The objectives of such study were twofold: (1) to evaluate the influence of changing only one process parameter (e.g. extruder screw speeed) upon the 3D-printed material properties and the structural response of the beams in a 4-point bending test, and (2) to develop a framework for quickly predicting the structural response for the first monotonic loading cycle of such material up to the damage initiation point using as input directly the material characterization test data.

2 PARTS, MATERIALS AND MANUFACTURING DETAILS

Three sets of carbon fiber filled thermoplastic PETG (PETG/CF) composite beams of monolithic cross-section were 3D-printed and loaded in a four-point bending test, up to complete failure. The material used for these SFRP structures was the Techmer/Electrafil 1711 3DP carbon fibre reinforced polyethylene terephthalate glycol (PETG/CF) with 30% carbon fibre by volume [1]. Figure 1 shows one such set of beams together with a corresponding material characterization box that was printed simultaneously. The print bead height and width were 5.08mm and 14.7mm, respectively, and the beams were 10 beads wide and 25 beads tall, resulting in overall dimensions of 1,830mm x 147.3mm x 127mm (L x W x H). Table 1 shows the average mass of each of the three sets of beams function of the extruder screw speed settings. Due to underextrusion of material, several bead interfaces in the Set A beams failed after a certain time following their removal from the print bed making those beams unsuitable for any subsequent tests. This phenomenon likely points to the long-term effects of viscoelasticity/creep on structures made of such materials, which will be the focus of future studies.

Figure 1: Set of three 3D-printed beams and material characterization box

Beam set	Extruder screw speed [rpm]	Beam mass [kg]
A	163	36.5
B	181	39.7
C	190	40.4

Table 1: Average 3D-printed beam set weight

3 EXPERIMENTAL TESTS

3.1 Four-point bending tests

All the SFRP beams were subject to loading in a 4-point bending test, up to failure. Figure 2 shows a typical setup before and after one of the tests. The load span was 0.61 meters, and the supports span was 1.63 meters. The structural supports as well as the load introduction elements consist of four High Density Polyethylene (HDPE) blocks. Three string-potentiometers (SP) were used to measure the beam deflection and six linear strain gauges (SG) were installed as in Figure 3 to measure the longitudinal strain developed during the test. Throughout the paper (1) or (11) is the longitudinal – or along-bead – direction, (2) or (22) is the transversal – or across-bead – direction, and (3) or (33) is the vertical – or bead-stack – direction.

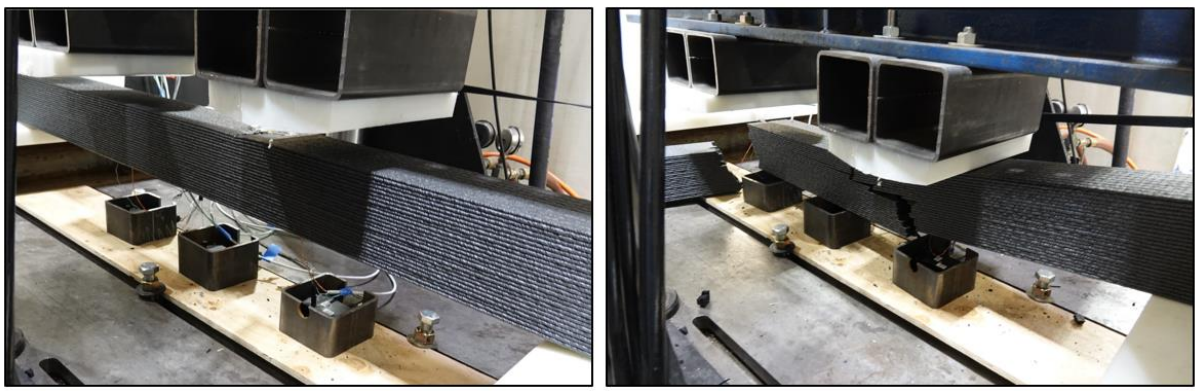

Figure 2: Four-point bending test setup: before and after test

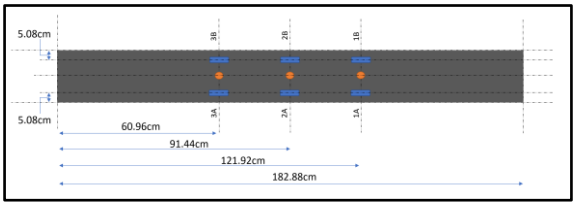

Figure 3: Instrumentation locations

Figure 4 shows the loadcell measured force vs. the deflection measured by the mid-span SP, for all beams, up to the failure load. It is remarkable the narrow grouping of both the force-displacement beam responses, as well as their failure loads (shown in Table 2). This was rather unexpected, signifying that the 5% variation in the extruder screw speed did not have any material impact in the flexural performance of the beams. The failure was brittle (i.e. with load dropping suddenly) for all the beams, with cracks propagating both along the bead interfaces as through the bead stack, as well as showing sometimes shear contribution (45° propagation).

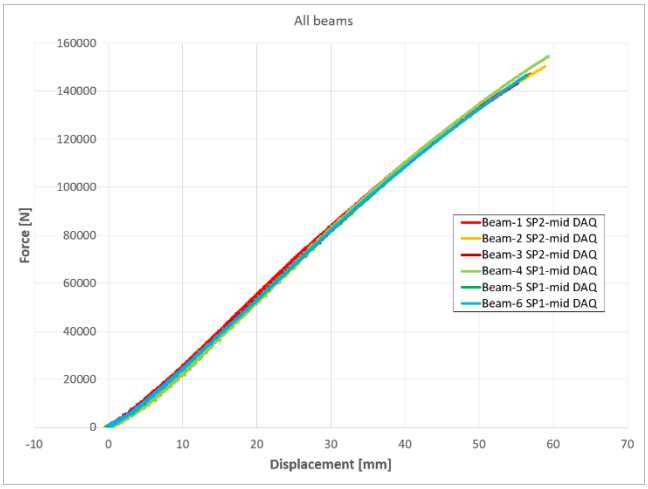

Figure 4: Force-Displacement responses for all beams, measured at midpoint

Beam	Extruder screw speed [rpm]	Failure load [kN]
Beam-1	181	147.3
Beam-2	181	150.3
Beam-3	181	143.2
Beam-4	190	154.3
Beam-5	190	146.9
Beam-6	190	146.0

Table 2: Failure loads for all beams

3.2 Material characterization tests

Coupons were cut from the purposely printed box for material characterization tests according to ASTM D638 (tensile test) [2] and ASTM D7078 (V-notched rail shear test) [3]. In the ASTM D638 test, the reported output is the longitudinal strain measured in the gauge region using a virtual extensometer

within the DIC system, while in the ASTM D7078 the reported output is the engineering shear strain measured using the DIC system as well. All material characterization tests were performed at the ASCC of UMaine and Figure 5 shows representative coupons for both types of tests. As the 3D-printing process results in in an orthotropic material, with carbon fibers aligning preferentially with the printing direction, tests were carried in both (11) and (33) directions.

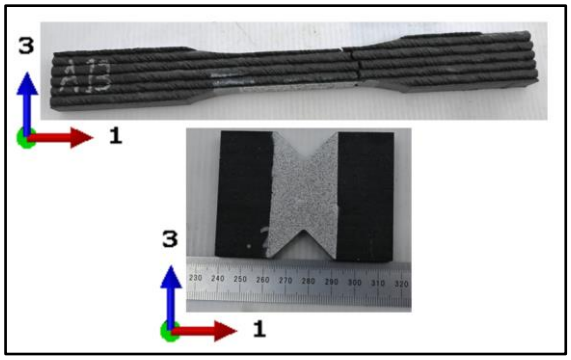

Figure 5: Tensile and Shear tests coupons, with DIC pattern

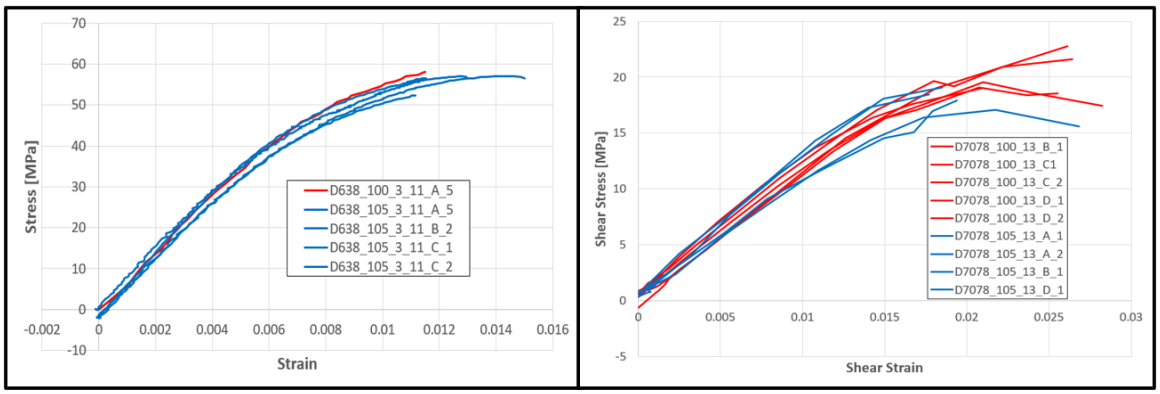

Figure 6: Stress-Strain responses: ASTM D638 (left) and ASTM D7078 (right)
181rpm (red) and 190rpm (blue)

Figure 6 reinforces the observation that there is not a significant difference in neither the tensile nor the shear response of the two batches of materials analyzed, while Table 3 summarizes the properties of this PETG/CF material.

Type of Test	Orientation	Ultimate Strength [MPa]	Modulus [GPa]	Strain at Failure [%]
Tension	11	58.0	7.1	0.93
	33	4.8	2.3	0.21
In-Plane Shear	13	20.6	1.2	2.73
	31	16	1.1	1.51

Table 3: Material properties PETG/CF

4 NUMERICAL MODELING

4.1 Material model

To capture the nonlinear response (see Figure 6) of the monotonic loading part of a virgin SFRP material up to the failure point, an elastic-plastic formulation was the obvious first choice. Abaqus FEA commercial software [4] offers the classical elastic-plastic model to which an anisotropic yield surface criterion was added (i.e. Hill quadratic potential) to capture the aforementioned tendency of the carbon fibres to align with the print direction. Table 4 shows the stiffness and strengths properties of an assumed transversely isotropic material model used in the simulations (a common assumption when modelling 3D-printed SFRP materials [5]-[6]). The compressive strengths ($S_{11}C$ and $S_{33}C$) were estimated based on a previously tested identical PETG/CF material [7] printed on a similar BAAM machine, for which the ratio of the ultimate compressive-to-tensile strength was 1.25 in (11) direction and 8.60 in (33) direction, respectively. The "Calibration" feature in Abaqus/CAE was used with a representative tensile test stress-strain response to get the material model yield stress (26.5 MPa) and the isotropic hardening curve.

PETG/CF properties	FEA input
E_{11}	7,100 MPa
E_{22}	2,300 MPa
E_{33}	2,300 MPa
ν_{12}	0.33
ν_{13}	0.33
ν_{23}	0.33
G_{12}	1,100 MPa
G_{13}	1,100 MPa
G_{23}	900 MPa
$S_{11}T$	58.0 MPa
$S_{11}C$	72.8 MPa
$S_{33}T$	4.8 MPa
$S_{33}C$	41.6 MPa
S_L	20.6 MPa

Table 4: PETG/CF properties used in FEA

It is worth mentioning here that characterizing the entire behaviour of a polymer material, i.e. load-unload behaviour, rate-dependence/viscoelasticity, damage onset and evolution, etc, was outside the scope of the current study, and would likely require pursuing of a different polymer-specific material modeling framework.

4.2 Simulating the coupon tests

To gain confidence in the material model used, the first step was to try to replicate the ASTM tensile and shear tests which will allow a direct comparison of the numerical model performance in those two simple loading scenarios. Both were modelled as displacement-controlled tests, using solid (continuum) elements with reduced integration (C3D8R). The material orientation convention in the FEA model is the same as shown for the coupons in Figure 5.

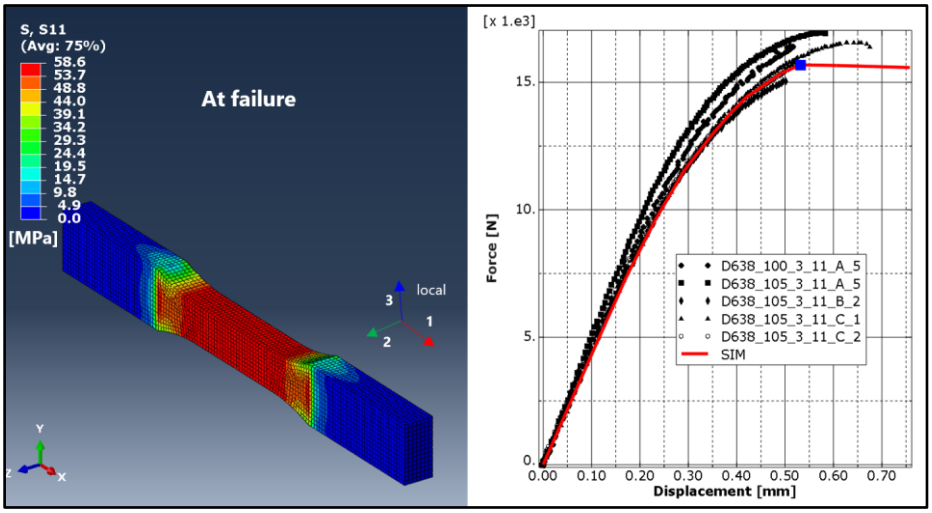

Figure 7: ASTM D638 response comparison

Figure 7 shows the very good correlation of the simulation and the tests' force-displacement response up to the point of failure (where the test force response drops to zero immediately after the peak, while the numerical material model diverges as it doesn't have any damage model incorporated). It can also be noted the good match between the longitudinal stress in the FEA model at the failure instant (58.6 MPa) and the ultimate tensile strength of the material (58.0 MPa). Similarly, Figure 8 shows the very good correlation between the simulation and the tests' "force vs. shear strain" response up to the failure point for the V-notch rail shear test, as well as the good match between the shear stress in the "notch" region of the FEA model (20.1 MPa) and the ultimate shear strength of the material (20.6 MPa).

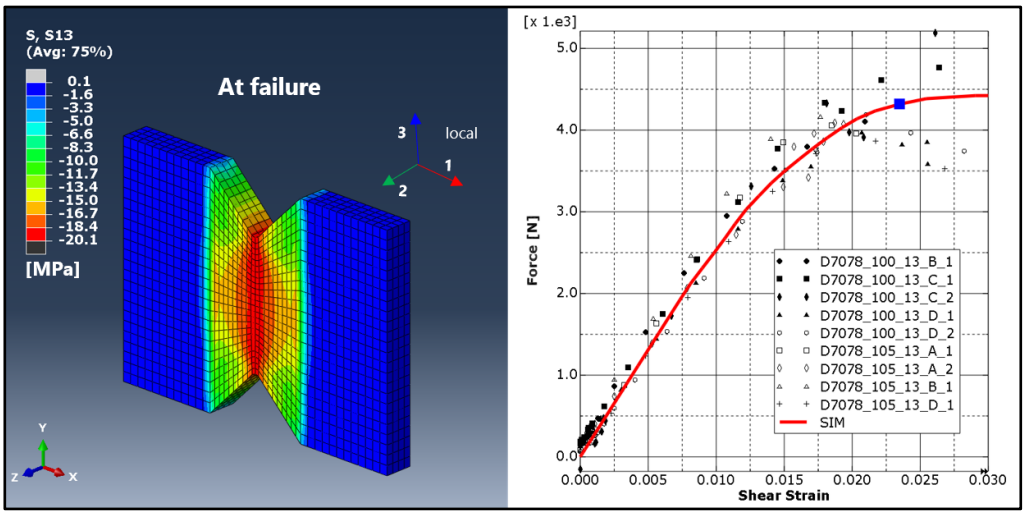

Figure 8: ASTM D7078 response comparison

4.2 Simulating the 4-point bending tests

A displacement-controlled static FEA was used to simulate the 4-point bending test of the full 3D-printed beam. Solid (continuum) elements with reduced integration and enhanced hourglass control (C3D8R) were used to model the structure. Figure 9 shows the transversely isotropic material orientations in the undeformed model.

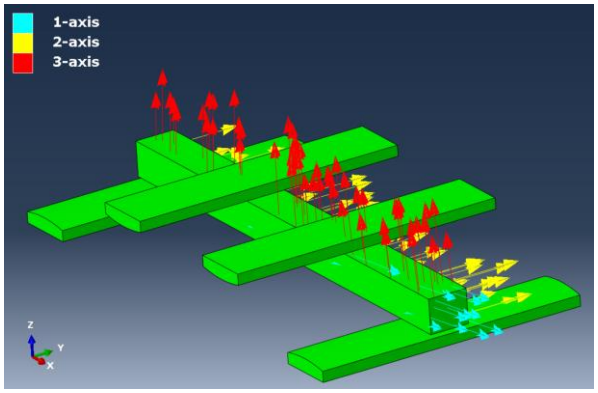

Figure 9: Material orientations in the FEA

Figure 10 shows the vertical deflection and the maximum principal stress in the FE model at beam failure, respectively. This latter predicted value of 58.7 MPa in tension corresponds very well with the material tensile strength of 58.0 MPa, reinforcing the experimental observation that the failure of the beam was initiated by the longitudinal tensile stress at its bottom.

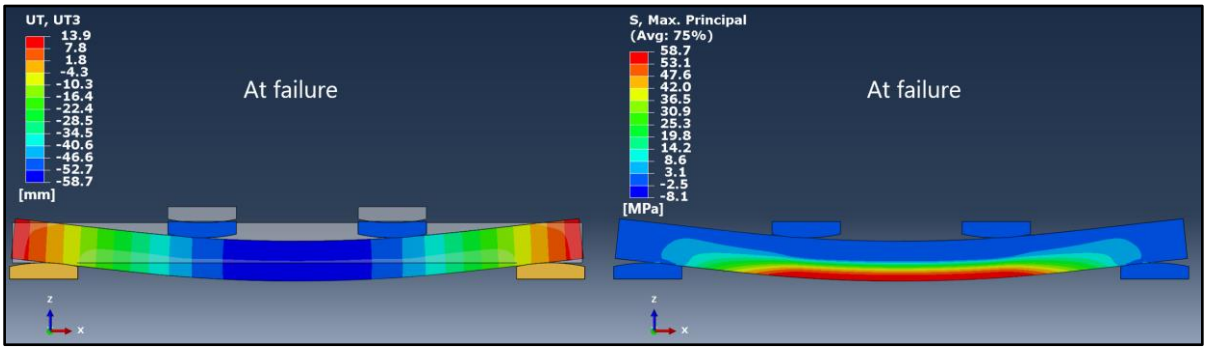

Figure 10: Vertical deflection (left) and max principal stress (right) in the FE model

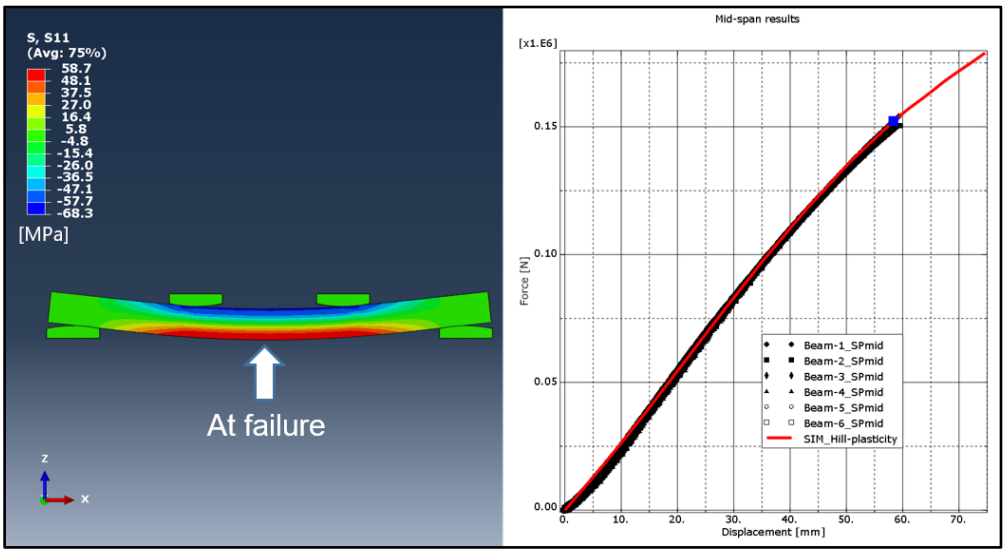

Figure 11: Longitudinal stress at failure (left) and force-deflection comparison with test data (right)

Figure 11 shows the longitudinal stress (S_{11}) in the FE model at the failure moment. According to this, the beam failure initiates at the bottom midspan where the longitudinal tensile stress exceeds the tensile strength of the material, while the compressive stress at the top is still somewhat lower than the compressive strength of the material (see Table 4). The predicted response of "force vs deflection" at the beam bottom midpoint in the FE model mimics very well the corresponding test results all the way up to the failure instant (again, with the observation that the FE model currently lacks a material failure mechanism, leading thus to subsequent diverging behaviour).

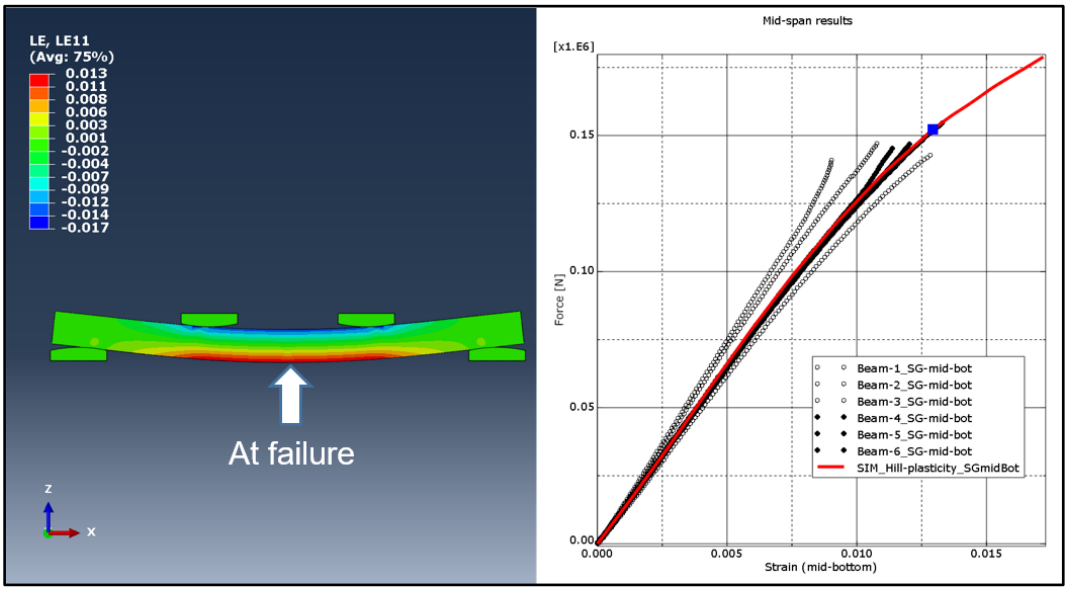

Figure 12: Longitudinal strain (right) and force-strain comparison with test (right)

Figure 12 shows the longitudinal strain in the FE model at the instant of failure, as well as the predicted "force vs longitudinal strain" response curve at the beam bottom midpoint compared with similarly located strain gauge responses in each of the beams tested. Despite some noticeable spread in the experimental measurements of the first batch of beams tested (beams 1, 2 and 3, i.e. the 181 rpm set), the FE simulation shows a good overall match with the strain gauge measurements for the whole loading curve up to the failure instant.

5 CONCLUSIONS

This paper presents a case study of a large-scale 3D-printed SFRP structural member (a beam) from which a couple of observations can be made. Firstly, it allows an initial understanding of the feasible limits in one of the key AM process parameters (e.g. extruder screw speed) within which no noticeable impact can be seen in the material response and corresponding structural performance. While unexpected, this fact can potentially be beneficial in terms of process robustness and confidence in structural predictions. Secondly, in the realm of numerical simulation, it was shown that using an elastic-plastic material model that includes an anisotropic yield criterion together with experimentally obtained material characterization data from coupon tests – essentially a so-called "blind prediction" – it is possible to mimic very well the response of this material in monotonic loading up to the failure point for several basic loading scenarios (tension, shear, bending).

ACKNOWLEDGEMENTS

The authors would like to acknowledge the Office of Naval Research (ONR) for sponsoring the work presented in this paper, through the "Composites for Advanced Maritime Structures" project number N00014-22-C-1086.

REFERENCES

[1] "Electrafil PETG 1711 3DP" Technical Datasheet, TechmerPM, Oct. 2020
[2] D20 Committee, "Standard Test Method for Tensile Properties of Plastics" ASTM International. doi: 10.1520/D0638-22
[3] D30 Committee, "Test Method for Shear Properties of Composite Materials by V-Notched Rail Shear Method" ASTM International. doi: 10.1520/D7078_D7078M-20E01
[4] ABAQUS Online User's Manual, 2022, https://www.3ds.com/products-services/simulia/
[5] S. Kim, H. Baid, A. A. Hassen, A. Kumar, J. Lindahl, D. Hoskins, C. Ajinjeru, C. Duty, P. Yeole, U. Vaidya, F. Abdi, L. Love, S. Simunovic, V. Kunc, "Analysis on Part Distortion and Residual Stress in Big Area Additive Manufacturing with Carbon Fiber-Reinforced Thermoplastic using Dehomogenization Technique", *CAMX Conference Proceedings*, Anaheim, California, September 23-26, 2019.
[6] M. Scapin, L. Peroni, "Numerical Simulations of Components Produced by Fused Deposition 3D Printing", *Materials* **2021**, 14, 4625, https://doi.org/10.3390/ma14164625
[7] C. Seigars, K. Warren, B. Steva, C. Murphy, B. Helten, "Characterizing the tensile and compressive behavior of PETG/CF and PC/CF manufactured using large-scale additive processes". *European Conference of Composite Materials (ECCM20)*, Lausanne, Switzerland, 2022.